

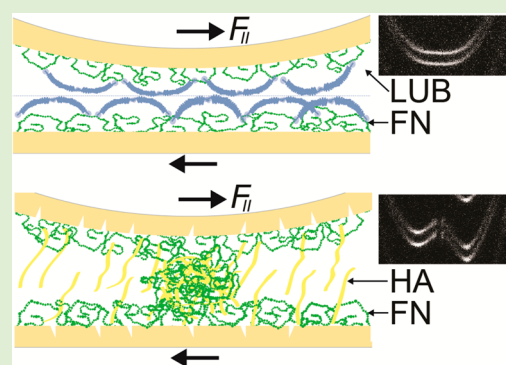
# Fibronectin mediates enhanced wear protection of lubricin during shear

Roberto C. Andresen Egiluz,<sup>†</sup> Sierra G. Cook,<sup>†</sup> Cory N. Brown,<sup>†</sup> Fei Wu,<sup>†</sup> Noah J. Pacifici,<sup>†</sup> Lawrence J. Bonassar,<sup>‡</sup> and Delphine Gourdon<sup>\*,†</sup>

<sup>†</sup>Department of Materials Science and Engineering and <sup>‡</sup>Department of Biomedical Engineering, Cornell University, Ithaca, New York, United States

## Supporting Information

**ABSTRACT:** Fibronectin (FN) is a glycoprotein found in the superficial zone of cartilage; however, its role in the lubrication and the wear protection of articular joints is unknown. In this work, we have investigated the molecular interactions between FN and various components of the synovial fluid such as lubricin (LUB), hyaluronan (HA), and serum albumin (SA), which are all believed to contribute to joint lubrication. Using a Surface Forces Apparatus, we have measured the normal (adhesion/repulsion) and lateral (friction) forces across layers of individual synovial fluid components physisorbed onto FN-coated mica substrates. Our chief findings are (i) FN strongly tethers LUB and HA to mica, as indicated by high and reversible long-range repulsive normal interactions between surfaces, and (ii) FN and LUB synergistically enhance wear protection of surfaces during shear, as suggested by the structural robustness of FN+LUB layers under pressures up to about 4 MPa. These findings provide new insights into the role of FN in the lubricating properties of synovial fluid components sheared between ideal substrates and represent a significant step forward in our understanding of cartilage damage involved in diseases such as osteoarthritis.



## INTRODUCTION

Healthy articular joints exhibit highly efficient lubrication and wear resistance over a person's lifetime. In synovial joints, cartilage surfaces slide past each other with friction coefficients as low as 0.0005–0.05<sup>1,2</sup> while being subjected to pressures up to about 20 MPa<sup>3</sup> imposed by wide gait and locomotion ranges. Although various mechanisms have been proposed to explain this extremely low friction under a large range of pressures and sliding speeds, no single model is able to give a satisfactory explanation. Therefore, cartilage lubrication is usually attributed to various lubrication modes, which include elasto-hydrodynamic, mixed, and boundary lubrication mechanisms.<sup>4–6</sup> The unique tribological properties of synovial joints arise from the combination of the porous cartilage structure<sup>7</sup> and the synergistic interactions of proteins present in the synovial fluid, which fill the cartilage pores.<sup>8</sup> In boundary lubrication mode, that is, at direct cartilage–cartilage contact, the outermost layer of the superficial zone of cartilage (Figure 1A) acts as a bearing surface during shear. The superficial zone also defines the interface between the cartilage and the synovial fluid (SF).<sup>9,10</sup> Moreover, it contains fibrillar proteins such as collagen type II (COL II)<sup>11,12</sup> and fibronectin (FN),<sup>13</sup> as well as large amounts of essential globular SF constituents that include lubricin (LUB),<sup>6</sup> phospholipids (PL),<sup>14,15</sup> hyaluronan (HA),<sup>13</sup> and serum albumin (SA)<sup>16</sup> (Tables 1 and 2). Although there have been numerous studies on (i) the individual contributions of SF components (LUB,<sup>17–19</sup> HA,<sup>20–22</sup>

PL<sup>15,23,24</sup>), (ii) the synergistic interactions between SF components (HA with LUB,<sup>25,26</sup> COL with LUB,<sup>27</sup> HA with PL,<sup>28</sup> HA with aggrecans<sup>29,30</sup>), and (iii) the role of SF<sup>31,32</sup> itself, the molecular mechanisms behind boundary lubrication at the superficial zone of cartilage in joints are still unclear. Previous studies found that LUB can strongly bind to COL II presenting different morphologies, which induces large repulsive interactions that increase with LUB concentration. On the other hand, although FN is known to play a crucial role in cell adhesion and protein–protein interactions when assembled into extracellular matrix fibers, its presence in the superficial zone and its role in lubrication have not been studied in detail.

HA, LUB, SA, and full SF have all been reported to exhibit unique tribological properties in boundary lubrication mode at biological and nonbiological interfaces.<sup>18,20,23,36–38</sup> SF has been shown to act as an effective boundary lubricant when confined either between opposing articular cartilage surfaces (using a variety of test configurations)<sup>37,39</sup> or between various nonbiological surfaces.<sup>36,37</sup> More recently, a friction study of nanometer-thick films of various mammalian SFs demonstrated that sheared SF layers physisorbed onto mica gradually aggregate in the shearing junction to form a homogeneous film resembling the lamina splendens, a gel-like layer covering

Received: June 17, 2015

Revised: July 27, 2015

Published: July 29, 2015

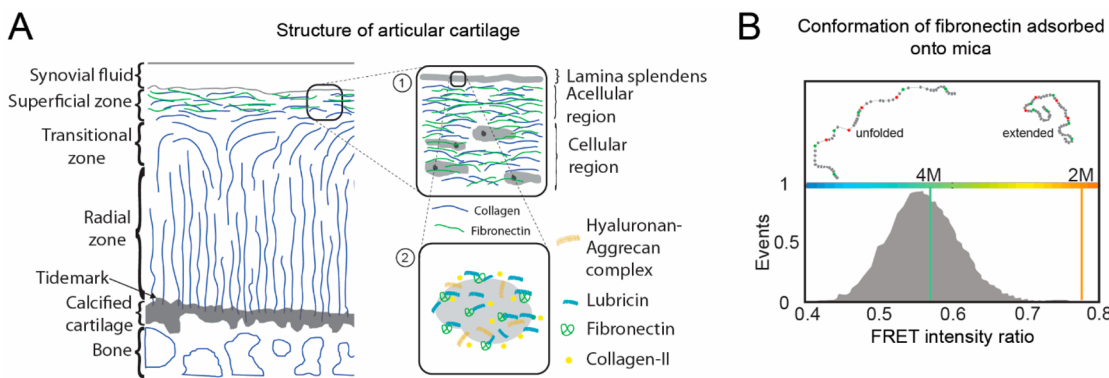


**Figure 1.** (A) Schematics of articular cartilage showing collagen type II fiber orientation as a function of depth. Inset 1: detail of the superficial zone of articular cartilage illustrating the cellular and acellular regions, and the presence of FN. Inset 2: representation of some relevant biomolecules present in the lamina splendens. (B) FRET intensity ratio frequency histogram of FN conformations, as measured by FRET-FN adsorbed onto curved mica substrates. Inset: Schematics of FN conformations suggested by FRET: most molecules are partially unfolded when adsorbed onto curved mica (calibration: 2 M corresponds to extended FN and 4 M corresponds to unfolded FN).<sup>51</sup>

**Table 1. Summary of the Main Abbreviations Used in This Manuscript and Their Corresponding Meanings**

abbreviation	meaning	abbreviation	meaning
AdG	Alexander-de Gennes	LR	long-range (forces)
BSA	bovine serum albumin	LUB	lubricin
COL II	collagen type II	MBI	multiple beam interferometry
ESF	equine synovial fluid	PBS	phosphate buffer saline
FN	fibronectin	PL	phospholipid
FRET	Förster resonance energy transfer	s	grafting distance
FRET-FN	FRET-labeled FN	SA	serum albumin
GAGs	glycosaminoglycans	SF	synovial fluid
GdnHCl	guanidine hydrochloride	SFA	surface forces apparatus
HA	hyaluronan	SMB	somatomedin
HEP	heparin	SR	short-range (forces)
HW	hard wall thickness	UHMWPE	ultrahigh molecular weight polyethylene
L	brush length		

**Table 2. Main Components Found in Human SF and Reported to Play a Role in Joint Lubrication**

component	molecular weight (kDa)	physiological concentration (mg/mL)	concentration used (mg/mL)
HA	1000	1–4 <sup>13,33</sup>	3
LUB	230	0.05–0.35 <sup>17</sup>	0.02
SA	66	8–11 <sup>16</sup>	8
PL	0.26	0.137 <sup>14,15</sup>	NA
GAGs	250	0.05–0.15 <sup>34</sup>	NA
FN <sup>a</sup>	440	0.3 <sup>35</sup>	0.3

<sup>a</sup>FN is found in synovial joints in its fibrillar, insoluble form when assembled into the extracellular matrix (cartilage) and in its soluble, globular form in SF.

the cartilage superficial zone and containing higher concentrations of the same essential components found in the SF.<sup>32</sup> The lubricating and wear protecting properties of HA have also been assessed at cartilage–cartilage<sup>6,40</sup> shearing junctions and nonbiological interfaces.<sup>21–23,36</sup> All these studies suggest that HA does not act per se as an effective boundary lubricant, but rather exhibits remarkable wear protection properties when grafted to or trapped between surfaces.<sup>20–23</sup> Furthermore, HA

wear protection was shown to be enhanced and accompanied by a reduction of the friction coefficient when LUB was present, even under high contact pressures.<sup>26</sup> This was attributed to the formation of HA-LUB aggregates that establish a protective cross-linked network.<sup>26</sup>

LUB alone was found to lubricate cartilage against cartilage,<sup>6,20,41</sup> cartilage against glass,<sup>42,43</sup> and latex against glass,<sup>44</sup> almost as efficiently as SF. Zappone et al. demonstrated that LUB physisorbed onto mica forms dense layers and exhibits friction coefficients as low as  $\mu = 0.02\text{--}0.04$  at low pressures (below 0.5 MPa), systematically increasing up to  $\mu = 0.2\text{--}0.6$  at higher pressures.<sup>18</sup> The friction properties of LUB are usually attributed to both the molecular architecture and the binding capability of the protein. LUB consists of a heavily glycosylated mucinous central domain (the lubricating domain) separating two globular domains (the binding domains).<sup>45</sup> LUB can bind to various articular cartilage and SF components, including COL II and HA. However, Elsaïd et al. showed that LUB's highest affinity is for fibrillar FN,<sup>46</sup> which is only present in the superficial zone of articular cartilage.<sup>13,47</sup> Finally, SA, which is present in SF at extremely high concentrations, was also reported to aid in the lubrication of artificial cartilage and to protect against wear when confined between ultrahigh-molecular-weight polyethylene (UHMWPE) and Al<sub>2</sub>O<sub>3</sub> or ZrO<sub>2</sub> surfaces in hip implants.<sup>38,48</sup> Similar to LUB, sheared SA can combine with HA to form structures that modify the tribological properties of SF and improve its lubrication.

While the contribution of collagen in joint tribology has been extensively studied, the role of FN remains unclear. FN is a multifunctional glycoprotein that is present both in the SF (in its globular form)<sup>49</sup> and in the superficial zone of cartilage (in its fibrillar form), but is lacking from the transitional or radial zones of cartilage (insets Figure 1A). We suggest that FN, which is expressed in abundance in the cartilage extracellular matrix near the articular surface,<sup>50</sup> is acting to directly bind LUB and subsequently facilitate localization of other SF components as well, such as HA.<sup>20,26</sup> In this work, we asked (i) whether FN is capable of binding SF components (such as LUB, HA, or SA), and (ii) whether such binding modifies the lubrication and wear protection of these components on ideal substrates. We used a Surface Forces Apparatus (SFA) to measure the normal and friction forces between thin films of SF components (or full SF) physisorbed onto FN-coated mica

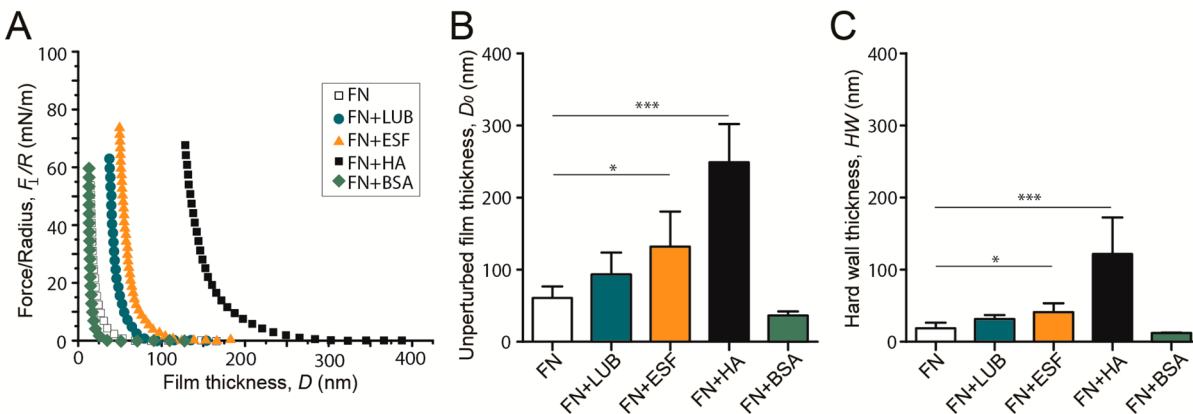


**Figure 2.** (A) Normal force  $F_{\perp}$  normalized by the surface radius of curvature  $R$  between SF layers physisorbed onto FN-coated mica as a function of the mica–mica surface separation distance,  $D$ . Forces were measured on approach in PBS without SF components (FN only, white squares), with LUB (FN+LUB, cyan circles), with full ESF (FN+ESF, orange triangles), with HA (FN+HA, black squares), and with BSA (FN+BSA, green diamonds). (B) Bar charts displaying the resulting average values of the unperturbed film thickness,  $D_0$  (onset of repulsion) and (C) average values of the compressed film thickness (“hard walls”)  $HW$  of the FN-coated mica surfaces before (white) and after incubation with SF components (cyan, orange, black, or green). For (B) and (C), values are reported as means + std dev,  $n = 4$ . In all cases,  $p < 0.05$  is indicated by a single star and  $p < 0.001$  by three stars.

surfaces, and we monitored the onset of surface damage upon load application and shear. Among all the configurations tested, FN-LUB tribosystems revealed the best tribological properties, exhibiting stable coefficients of friction ( $\mu = 0.23$ ) and efficient protection of the shearing surfaces against abrasive wear, under contact pressures up to 4 MPa.

## MATERIALS AND METHODS

**Preparation of FN Surfaces and FRET Analysis of FN Conformation.** Soluble plasma FN (Sigma-Aldrich, MO, U.S.A.) was allowed to adsorb onto mica for 1 h (50  $\mu$ L of FN solution in phosphate buffer saline (PBS) at 0.3 mg/mL incubated at room temperature). Förster Resonance Energy Transfer (FRET) labeling of FN was used to analyze FN conformations at the mica surface following a previously published protocol.<sup>51</sup> Briefly, FN molecules were labeled for intramolecular FRET with both AlexaFluor 488 and AlexaFluor 546 (Invitrogen, CA, U.S.A.). Calibration of soluble FRET-labeled FN (FRET-FN) was carried out in a guanidine hydrochloride (GdnHCl) denaturant solution at concentrations of 0 M (compact FN), 2 M (extended FN), and 4 M (unfolded FN) to obtain acceptor/donor (FRET) intensity ratios ( $I_A/I_D$ ) as a function of protein denaturation.<sup>51</sup> GdnHCl calibrations are indicated by the green (4 M) and orange (2 M) vertical lines in the histogram shown in Figure 1B. To perform FRET analysis, FN-coated mica surfaces were prepared by incubating 100  $\mu$ L of FN solutions (50  $\mu$ g/mL) containing 10% FRET-FN and 90% unlabeled FN onto mica surfaces glued on SFA silica discs (see next section). Incubated surfaces were stored at 4 °C for 24 h, then rinsed three times and kept immersed in PBS. Samples were imaged for FRET with a Zeiss 710 confocal microscope using a water-immersion 40× objective.

**Surface Forces Apparatus.** A SFA-Mark III (SurForce, LLC, Santa Barbara, CA, U.S.A.) was used to measure the normal and friction forces between layers of SF components physisorbed onto FN-coated mica surfaces. Two freshly cleaved atomically smooth back-silvered mica (S&J Trading, Australia) sections were glued onto half cylindrical silica discs ( $R = 1$  cm) with UV curing glue (Norland 61, Cranbury, NJ, U.S.A.). The discs were mounted in a cross-cylindrical geometry, and the absolute separation distance,  $D$ , was measured in real time via multiple beam interferometry (MBI).<sup>52,53</sup> MBI was also used later to quantify the onset of damage of the shearing surfaces. Mica-mica contact in air was first determined to set the reference distance,  $D = 0$ , prior to each surface functionalization. For normal force measurements, the lower surface was mounted onto a horizontal double cantilever spring ( $k_N = 590$  N/m) and displaced at 5 nm/s using a step

motor to avoid large viscous effects and ensure exclusive assessment of quasi-static (equilibrium) interactions. For friction force measurements, the lower surface was mounted onto a stiffer horizontal spring ( $k_N = 1650$  N/m) for achieving higher pressures, and the upper surface was mounted onto a vertical double cantilever spring ( $k_L = 700$  N/m) holding semiconductor strain gauges to assess lateral forces. Shearing was achieved via a ceramic bimorph slider, and shearing velocities of 0.3, 3, and 30  $\mu$ m/s were used, which correspond to the range of boundary lubrication modes achieved during light physical activity (such as walking). MBI fringes of equal chromatic order were collected with an SP2300 photospectrometer (Princeton Instruments, NJ, U.S.A.) with a 600 g/mm grating and 500 nm blaze, digitalized with a ProEM CCD camera (Princeton Instruments, NJ, U.S.A.), and visualized using Lightfield v4.0 (Princeton Instruments, NJ, U.S.A.). Friction traces were acquired and analyzed with a NI USB-6210 and LabView v8.6 (National Instruments, Austin, TX, U.S.A.), respectively.

**Preparation of SF Components Layers Physisorbed onto FN-Coated Mica.** All physisorbed SF components layers were prepared using the same protocol unless otherwise indicated. First, 50  $\mu$ L of bovine serum albumin (BSA) at 0.02 mg/mL was added to FN-coated mica surfaces for 30 min to block nonspecific interactions, and rinsed with PBS. Finally, the resulting FN-coated mica surfaces were incubated for 1 h with 50  $\mu$ L of either ESF (as extracted from equine carpus joint), HA (1 MDa; Lifecore Biomedical, San Diego, CA, U.S.A.) in PBS (3 mg/mL), or BSA (Sigma-Aldrich, MO, U.S.A.) in PBS (8 mg/mL). LUB (recombinant human lubricin) was a gift of Dr. Carl Flannery of Wyeth Laboratories) layers were obtained by incubating FN-coated mica overnight with 50  $\mu$ L of a more dilute solution of LUB in PBS (0.02 mg/mL). This subphysiological LUB concentration corresponds to the value at which the friction coefficient  $\mu$  was reported to become independent of LUB concentration.<sup>43</sup> After incubation, the samples were thoroughly rinsed with PBS. All functionalization steps mentioned above were carried out on mica surfaces already mounted in the SFA, which was placed in a laminar flow cabinet to prevent particle contamination. All normal and friction experiments were performed in PBS at 25 °C.

The experiments were performed in agreement with the procedures and guidelines provided by the biosafety committee at Cornell University.

## RESULTS

**Conformation of FN Adsorbed onto Curved Mica as Determined by FRET.** To investigate the conformation of FN adsorbed onto SFA curved ( $R = 1$  cm) mica surfaces, we used

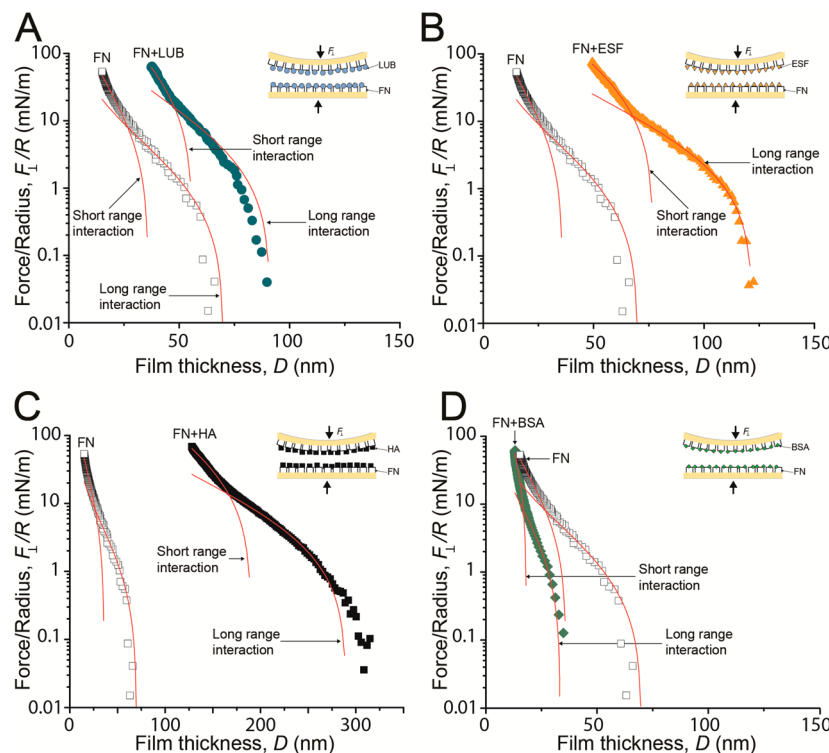


**Figure 3.** Semilog plots of representative curves of the normal force  $F_{\perp}$  normalized by the surface radius of curvature  $R$  as a function of the film thickness  $D$ . (A) LUB (cyan circles), (B) ESF (orange triangles), (C) HA (black squares), and (D) BSA (green diamonds) adsorbed to FN-coated mica. White squares in each panel represent FN only. Red lines indicate AdG fits to eq 1. Insets in each panel indicate flat on sphere contact configuration of mica substrates coated with FN (white squares) and corresponding SF components (A, C, D) or ESF (B), as well as acting force vectors.

FRET labeled FN and calculated the average FRET ratios of various fields of view at the surface<sup>51</sup> (Figure 1B). Our data indicate a relatively low FRET intensity ratio (0.53), suggesting that most FN molecules are unfolded when adsorbed onto curved mica, losing at least partially their tertiary/secondary structure (as indicated in Figure 1B).

**Normal Forces between SF Layers Physisorbed onto FN-Coated Mica.** To determine whether FN acts as a tethering molecule between ideal surfaces and SF components, we used the SFA to measure the normal forces between SF components (such as LUB, HA, or SA) and full ESF layers when physisorbed onto FN-coated mica surfaces. LUB concentration was chosen as the value at which the friction coefficient  $\mu$  had been previously reported to become independent of LUB concentration,<sup>43</sup> whereas HA and BSA concentrations were set at physiological values. Figure 2A displays normal forces, reported as  $F_{\perp}/R$ ,  $F_{\perp}$  being the normal force and  $R$  the surface radius of curvature, between (i) LUB, (ii) ESF, (iii) HA, and (iv) BSA layers adsorbed to FN-coated mica. For comparison, a  $F_{\perp}/R$  profile of FN-coated mica without SF component is also shown. In all cases, the interaction forces were systematically repulsive (no adhesion between surfaces). Only forces on approach are displayed as no hysteresis between interactions upon approach and separation was measured, except in the case of HA, where a small hysteresis was detected, as previously reported for high molecular weight polymers<sup>23,26</sup> (data not shown).

Unperturbed film thickness ( $D_0$ ) was assigned as the onset of repulsion measured on approach (it was precisely extracted from the long-range Alexander-de Gennes fit, as explained in the next section). Figure 2B displays  $D_0$  before (only FN) and

after incubation with either LUB, ESF, HA, or BSA. A bare FN film is shown as a reference, showing a film thickness  $D_0$  of  $61 \pm 16$  nm. After LUB, ESF, and HA incubation,  $D_0$  increased to  $94 \pm 30$ ,  $132 \pm 49$ , and  $249 \pm 53$  nm, respectively. Because our measurements were made after the surfaces were thoroughly rinsed with PBS, these variations of  $D_0$  indicate that FN tethers LUB, ESF, and HA to mica. In contrast, incubation with BSA resulted in a decrease of  $D_0$  down to  $37 \pm 7$  nm, suggesting either an exchange of FN with BSA molecules or a collapse of the whole FN+BSA film.

Figure 2C reports average film thicknesses measured under the maximum load applied in our experiments (or “hard wall” thicknesses, HW). HW values trend resembled that of initial thicknesses  $D_0$ . Bare FN films showed an average HW of  $19 \pm 7$  nm, increasing to  $31 \pm 6$ ,  $41 \pm 12$ , and  $122 \pm 51$  nm after incubation with LUB, ESF, and HA, respectively. Here too, incubation with BSA resulted in a thinner film, with HW decreasing to  $12 \pm 1$  nm. Collectively, these data indicate that FN is able to tether the selected SF components to mica strongly enough to prevent them from being expelled from the contacting surfaces, even when the junction is subjected to high compressive forces.

**High Repulsion Provided by Brush-Like Behavior of SF Physisorbed Layers in Salty Media.** To understand the origin of the repulsive interactions reported above, semilog plots of the force–distance profiles shown in Figure 2A were fitted with the Alexander-de Gennes (AdG, eq 1) model. The choice of this theory ordinarily used to describe grafted neutral polymer brushes, rather than a more complex charged polyelectrolytes model, is justified by the high salt content of the medium (PBS, ionic strength 150 mM), which screens most

of the electrostatic interactions between protein domains/chains. The equation describing the interactions of such so-called “brush-like” systems is<sup>54</sup>

$$\frac{F_{\perp}(D)}{R} = \frac{16\pi k T L}{35 S^3} \left[ 7 \left( \frac{2L}{D} \right)^{4/5} + 5 \left( \frac{D}{2L} \right)^{7/4} - 12 \right] \quad (1)$$

where  $k$  is the Boltzmann constant,  $T$  is temperature, and the fitting parameters  $L$  and  $s$  are the equilibrium brush length and average grafting spacing, respectively. The applicability of the AdG model to describe SF components at the superficial zone of cartilage has been suggested in previous studies.<sup>18,32,55,56</sup> However, the observed agreement between our experimental data and the AdG theory does not necessarily imply that the SF components would adopt a well-defined dense brush conformation on the mica substrate; it rather suggests that the protein/polyelectrolyte films adsorbed on the surfaces can be described as a purely repulsive effective brush layer.

Figure 3 combines representative experimental and fitted (red lines) data. All systems (Figure 3A–D) showed two clear regimes, a long-range and a short-range interaction, both of which were well fitted with the AdG model. As a control, we measured ESF and BSA without underlying FN, which were also well fitted by the AdG model (Figure S1). Fitting values corresponding to effective grafting density ( $s$ ) and brush equilibrium length ( $L$ ) for both long-range (LR) and short-range (SR) interactions, extracted for all systems, are summarized in Table 3.

**Table 3. Effective Brush Lengths ( $L$ ) and Average Grafting Distances ( $s$ ) for Long-Range (LR) and Short-Range (SR) Interactions Obtained from Eq 1**

component	$L_{LR}$ (nm)	$s_{LR}$ (nm)	$r^2$	$L_{SR}$ (nm)	$s_{SR}$ (nm)	$r^2$
FN	35	6.0	0.98	18	2.5	0.98
FN+LUB	46	4.1	0.97	28	1.7	0.98
FN+ESF	61	5.7	0.99	39	2	0.99
FN+HA	146	5.8	0.99	95	2.5	0.98
FN+BSA	17	3.8	0.98	9	1.1	0.92
LUB <sup>a</sup>	65	14	0.90	NA	NA	NA
LUB <sup>b</sup>	115	14	0.89	NA	NA	NA
ESF	35	2.3	0.98	22	1	0.99
BSA	28	2.6	0.85	17	1	0.99

<sup>a</sup>At a concentration of 0.064 mg/mL. <sup>b</sup>At a concentration of 0.290 mg/mL, both obtained from ref 18. NA = not available.

Although the fits of FN+LUB, FN+ESF, and FN+HA repulsive interactions (Figure 3A–C) indicated larger brush lengths  $L$  than FN films alone, FN+BSA measurements (Figure 3D) revealed shorter  $L$  values than FN alone. For ESF without underlying FN, long-range and short-range  $L$  values decreased by one-half compared to FN+ESF. Finally, for BSA without underlying FN, long-range and short-range values doubled when compared to FN+BSA. Collectively, the high reversible repulsions reported suggest that, in a medium of high salinity, SF components can be described as a repulsive effective brush layer adsorbed onto the mica surface, preventing interpenetration of opposite layers when pressed against each other, even under high pressures (see Discussion).

**Lubrication and Enhanced Wear Protection of Mica Surfaces Provided by FN-Tethered SF Layers.** Next, we asked whether the presence of FN improves the lubrication of

SF layers and contributes to the protection of the shearing surfaces against damage. We used the SFA to monitor both the friction forces  $F_{\parallel}$  (at various pressures and shearing velocities) and the onset of surface damage between FN-tethered LUB, ESF, HA, and BSA layers subjected to shear in PBS at 25 °C (Figure 4). Figure S2 shows control experiments using ESF and BSA without underlying FN. Film pressures were obtained from the Derjaguin approximation for a cross-cylindrical geometry.<sup>54</sup>

$$P = -\frac{\partial W}{\partial D} = -\frac{1}{2\pi R} \left( \frac{\partial F_{\perp}}{\partial D} \right) \quad (2)$$

where  $W$  is the interaction energy  $W = F_{\perp}/2\pi R$ ,  $D$  is the film thickness or absolute separation distance, and  $R$  is the surface radius of curvature. Both maximum applied pressures (when no wear was observed) and pressures at onset of wear are summarized in Table 4. The use of the Derjaguin approximation was motivated (i) by the range of separation distances investigated, which was much smaller than the radius of curvature of the silica cylinders used to hold mica surfaces and (ii) by the fact that flat contact was usually not achieved at the onset of wear, that is, when  $P_{\text{wear}}$  was determined.

The friction forces  $F_{\parallel}$  measured for FN+LUB (Figure 4A) (i) depended linearly on the normal force,  $F_{\perp}$ , vanishing at  $F_{\perp} = 0$  and (ii) increased slightly with shearing velocity  $V_{\text{shear}}$ . It is worth noting that no surface damage was detected in these experiments (as illustrated in Figure 5A–C by smooth MBI fringes), which indicates that FN+LUB ensured both effective lubrication ( $\mu = 0.2–0.3$ ) and most importantly protection of the surfaces against wear at pressures up to 14 MPa at the highest tested velocity, that is, well above the physiological range.

The friction forces  $F_{\parallel}$  measured on FN+ESF were found to (i) depend linearly on the applied normal load,  $F_{\perp}$ , vanishing at  $F_{\perp} = 0$ ; however, they were (ii) independent of shearing velocities (Figure 4B). Although the FN+ESF combination exhibited a higher coefficient of friction ( $\mu = 0.52 \pm 0.015$ ) than the FN+LUB tribosystem, it also efficiently protected the surfaces from damage under contact pressures up to about 10 MPa at the highest tested velocity.

In contrast, high friction coefficients and early damage were consistently observed while shearing FN+HA layers (Figure 4C), in particular, at the lowest shearing velocity ( $V_{\text{shear}} = 0.3 \mu\text{m/s}$ ). At this speed the coefficient of friction did not depend linearly on applied load  $F_{\perp}$  and did not vanish at  $F_{\perp} = 0$ , suggesting slight shear-induced adhesion in the system. Unlike FN+LUB and FN+ESF, shearing FN+HA was systematically accompanied by surface wear (starting at low pressure) leading to a decrease of the friction coefficient.

The friction forces  $F_{\parallel}$  measured on FN+BSA were found (i) to depend linearly on the applied normal load  $F_{\perp}$  and vanish at  $F_{\perp} = 0$  and (ii) to be weakly sensitive to shearing velocity (Figure 4D). The wearless friction coefficient was found to be  $\mu = 0.44 \pm 0.06$ , and damage appeared at pressures of  $P \approx 1.2$  MPa, which decreased  $\mu$  to  $0.28 \pm 0.025$ . Despite reports indicating that human SA properly lubricates artificial joints when adsorbed onto hydrophilic (ceramic) surfaces,<sup>38</sup> we observed poor lubrication and wear protection even at low loads. The friction variations measured across HA and BSA films are characteristic of a transition from a smooth (high friction coefficient) adhesion-controlled to a rough (lower friction coefficient) wear-controlled frictional regime.

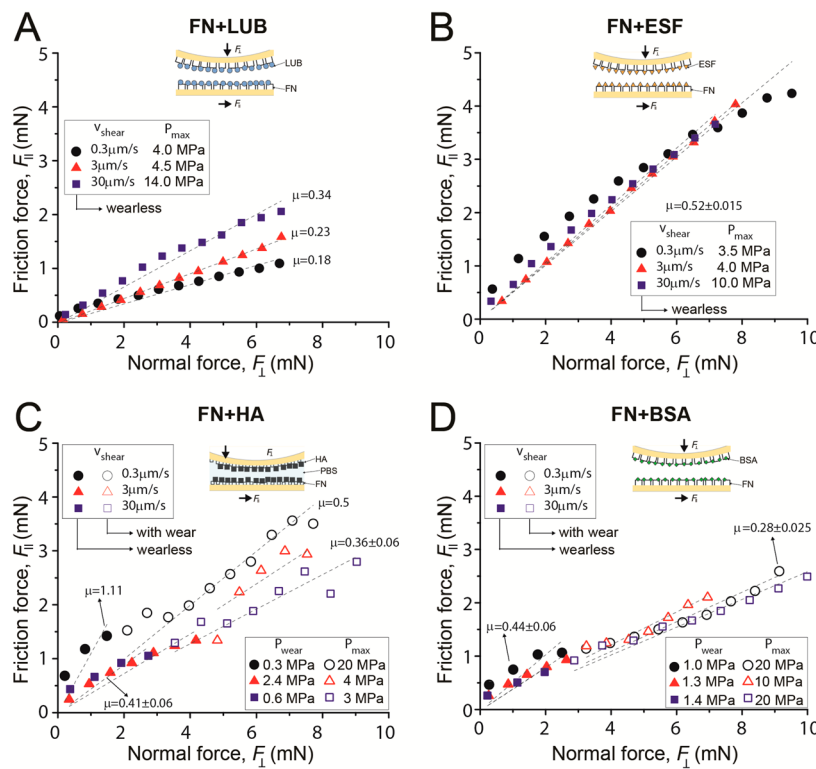


**Figure 4.** Friction force  $F_{\parallel}$  as a function of normal force  $F_{\perp}$  between (A) mica surfaces with adsorbed FN and LUB, (B) with adsorbed FN and ESF, (C) with adsorbed FN and HA, and (D) with adsorbed FN and BSA all sheared in PBS. The surfaces were sheared at sliding velocities of  $V = 0.3 \mu\text{m/s}$  (black circles),  $V = 3 \mu\text{m/s}$  (red triangles), and  $V = 30 \mu\text{m/s}$  (blue squares). Open symbols for HA and BSA indicate measurements after the surfaces became damaged. Insets in each panel indicate flat on sphere contact configuration of mica substrates coated with FN (white squares) and corresponding SF components (A, C, D) or ESF (B), as well as acting force vectors.

**Table 4. Pressures Reported at Onset of Wear; In Parentheses: Maximum Applied Pressures without Sign of Wear**

component	$P_{\text{wear}}$ (MPa)			$P_{\text{wear}}$ (MPa) from literature
	$V = 0.3 \mu\text{m/s}$	$V = 3 \mu\text{m/s}$	$V = 30 \mu\text{m/s}$	
FN+LUB	(4)	(4.5)	(14)	NA
FN+ESF	(3.5)	(4)	(10)	NA
FN+HA	0.3	2.4	0.6	NA
FN+BSA	1	1.3	1.4	NA
LUB	NA	NA	NA	0.4 (at $V_{\text{shear}} = 1 \mu\text{m/s}$ ) <sup>a</sup>
HA	NA	NA	NA	0.4 (at $V_{\text{shear}} = 10 \mu\text{m/s}$ ) <sup>b</sup>
ESF	0.9	1.0	1.5	NA
BSA	0.60	0.73	0.47	NA

<sup>a</sup>From ref 18. <sup>b</sup>From ref 23; NA = not available.

**Monitoring Surface Damage via Multiple Beam Interferometry (MBI) Spectroscopy.** The SFA relies on optical interferometry, which allows us to monitor the onset of damage in the shearing junction in real time. While shape changes of the interference fringes are linked to changes in the shape and size of the contacting junction, intensity alterations reflect changes in (i) refractive index of the confined medium (visible in even fringes) and (ii) obstruction of the light by wear-generated surface debris (visible in both odd and even fringes). Figure 5 shows a sequence of fringes illustrating the starting (low pressure) and ending (high pressure) points in our shearing experiments of FN+LUB, FN+ESF, FN+HA, and

FN+BSA, at all three shearing velocities. Although FN+LUB fringes flattened upon load application, no major intensity changes were measured, indicating that neither surface wear nor material accumulation occurred even under high pressure (Figure 5A–C). In the case of FN+ESF, a local change in the intensity of the even fringes (red arrows in Figure 5D,E) signaled material accumulation at the edges of the junction, that is, shear-induced formation of aggregates in the FN+ESF layer. Similar observations have been reported while shearing pure SF between mica surfaces in PBS.<sup>32</sup> This shear-induced phenomenon has been suggested to be a mechanism for the formation of the lamina splendens. ESF accumulation rather than damage to the underlying mica was indicated by intact odd fringes at all pressures and shearing velocities (Figure 5D–F) and later confirmed by direct visualization of the mica surfaces (post shearing) using a microscope objective (no wear track visible, data not shown).

In contrast, damage was observed on FN+HA surfaces, as indicated by double yellow arrows pointing at both odd and even fringes (Figure 5G–I). Monitoring the fringes over time showed that the surfaces would gradually deform, peel off the HA film, and form debris that eventually incorporated mica flakes. Figure S3 describes in detail the evolution of contact shape and wear debris size upon shearing. Mica damage was characterized by a single “wear track”, as confirmed after shearing using a microscope objective (data not shown). These results suggest that FN tethers HA molecules only weakly to mica: enough to retain HA in the junction during compression but not enough to be sheared over large distances. In fact, the poor wear resistance of HA has been reported to improve when

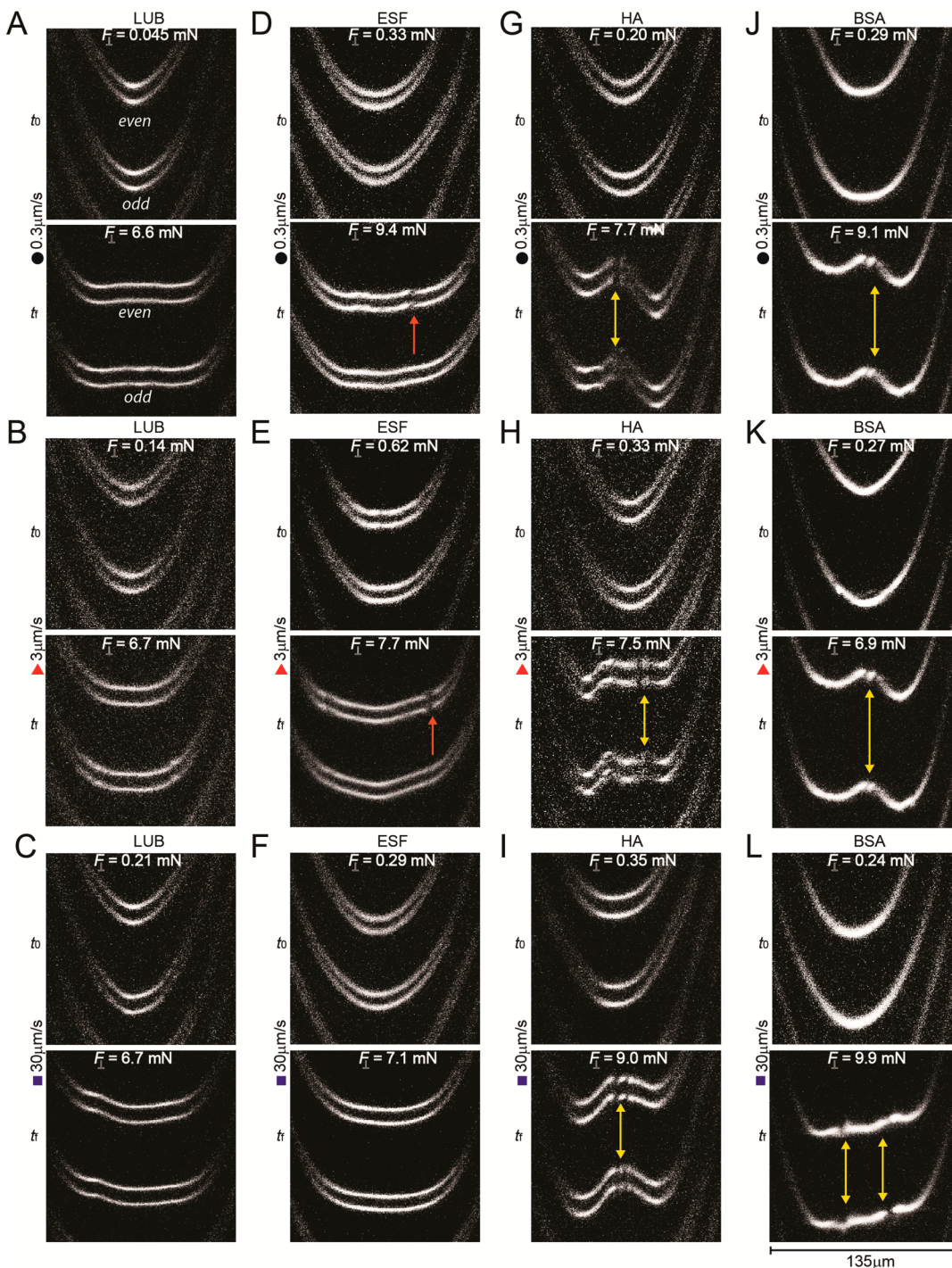


**Figure 5.** MBI visualization of representative mica surfaces coated either with FN+LUB films (A–C), FN+ESF films (D–F), FN+HA films (G–I), or FN+BSA films (J–L) at the beginning ( $t_0$ ) and the end ( $t_f$ ) of shear application, at various sliding velocities. Film agglomeration (without surface damage) is indicated by single-sided red arrows pointing at even fringes, while mica surface damage is signaled by double-sided yellow arrows pointing at both odd and even fringes. All panels show odd fringes at the bottom and even fringes on top, as indicated in panel (A).

molecules are chemically grafted to mica before shearing.<sup>23</sup> Finally, FN+BSA showed similar early damage of the surfaces, as illustrated by double yellow arrows in Figure 5J–L.

**Particulate Formation.** Figure S3 shows the formation and evolution of wear particles in the shearing junction as a function of normal applied load  $F_{\perp}$  at all shearing velocities (Figure S3). Our data confirm that damage of FN+HA and FN+BSA films start at significantly low loads. As neither the HA nor the BSA film creates a sharp (smooth) interface when adsorbed onto

opposing mica surfaces, shearing likely causes them to detach and build up aggregates, leaving behind mica regions entirely unlubricated. This then leads to the release of mica flakes (particles) responsible for the rapid propagation of abrasive wear throughout the entire shearing junction.

## DISCUSSION

Our quasi-static normal force data indicate that FN strongly tethers SF components to underlying mica surfaces, as

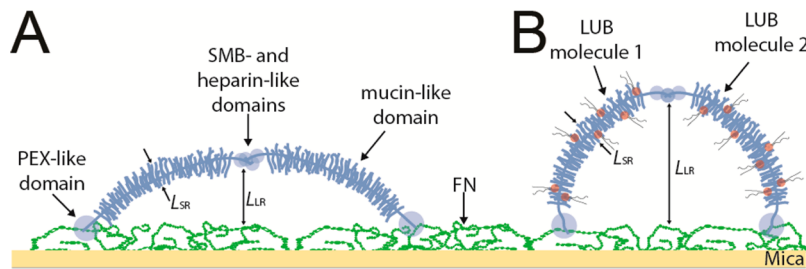


**Figure 6.** Proposed dimer configurations of (A) LUB at low concentrations and (B) LUB at high concentrations (as found in SF when they are likely decorated with PL).

evidenced by reversible long-range repulsive interactions measured in all films when pressed against each other. SF is composed of a complex mixture of lipids, proteins and polyelectrolytes. These SF components are unlikely to adopt a perfect brush conformation when adsorbed at the superficial zone of articular cartilage. However, as reported in other SF studies,<sup>18,32,55,56</sup> the agreement between our normal force measurements on FN+SF films and the AdG theory suggests that the films adsorbed onto mica can be described as purely repulsive effective neutral brush layers. Additionally, our friction measurements demonstrate that, among all individual SF components studied, FN and LUB act synergistically to ensure the best lubrication (i.e., the lowest friction forces and friction coefficients among all tested conditions) and to provide the most efficient protection of the shearing surfaces against abrasive wear.

**FN Conformation and Its Role in Tethering SF Components.** FN is known to adopt a variety of conformations depending on physical (curvature,<sup>57</sup> strain<sup>51,58</sup>) and chemical (pH,<sup>51</sup> charge<sup>59</sup>) factors, which determine its degree of unfolding and the availability of its binding sites for other proteins (and/or cells). FN was found to adopt a partially unfolded conformation when forming monomolecular films adsorbed onto curved mica substrates, as indicated by low FRET intensity ratios (Figure 1B). This suggests that many of the cryptic binding sites present on FN (sites usually buried within folded type III modules) might be already exposed.<sup>51</sup> The two repulsive regimes (long-range and short-range) identified in FN films could be attributed to the secondary and/or tertiary structure present in FN. Although our FRET data indicate unfolding of the weakest (mechanically unstable) FN type III (FN-III) modules, the rest of the molecule consists of more stable (disulfide bond-stabilized) type I (FN-I) and type II (FN-II) domains that can be described as a repulsive effective brush.<sup>60</sup> Short-range repulsion could then be explained by the reorientation of these FN-I and FN-II domains forced to lay down onto the mica surface. For example, FN-I<sub>4</sub> and FN-I<sub>5</sub> have unit cell lengths of  $a = 9$  nm,  $b = 4$  nm, and  $c = 7$  nm,<sup>61</sup> which compare well with the measured  $L_{SR}$ . Cartilage is highly porous and, therefore, a complex system to decipher surface phenomena. One of the advantages of using mica is that it is atomically smooth and nonporous, which reduces the complexity of the system by ensuring that all measured changes in the interfacial fluid are occurring between rather than within the sheared surfaces. In the superficial zone of cartilage, however, FN is present in its fibrillar form<sup>13</sup> (as opposed to our simplified model consisting of a monomolecular film of FN), so it is very likely that FN conformations vary as a function of fiber strain, which itself is set by the level of compression and shear of the cartilage surfaces. Such strain-induced newly exposed

cryptic sites on FN<sup>58,62</sup> will consequently control the binding of specific surface-active molecules (such as LUB, HA, and PL) and likely enhance wear protection.

FN has exposed heparin (HEP) binding domains both at the amino terminus (located on FN-I<sub>1–5</sub>) and close to the carboxyl terminus (located on FN-III<sub>12–14</sub>).<sup>63</sup> These sites could serve as binding domains for the positively charged somatomedin (SMB) and HEP binding domains present on LUB.<sup>64</sup> However, reduction and alkylation are known to reduce the ability of LUB to bind to the cartilage surface,<sup>45</sup> suggesting that LUB likely utilizes its PEX-like domain (C-terminus)<sup>45</sup> to bind to cartilage and its SMB- and heparin-like domains to self-aggregate into dimers.<sup>18,19,45</sup> Considering that LUB binds to FN via its C-terminus and self-aggregates via its N-terminus (Figure 6), loop-loop interactions would then lead to brush-mediated long-range repulsion, while short-range repulsive interactions would arise from the steric hindrance between the oligosaccharides comprising the dense side chains of the mucin-like LUB domain. Such dimeric LUB loop interactions could indeed account for the 10 nm increase of both  $L_{LR}$  and  $L_{SR}$  values for FN+LUB layers when compared to FN alone.

FN+ESF layers show a force-distance dependency very similar to that obtained for FN+LUB layers, (with a 15 nm increase for both  $L_{LR}$  and  $L_{SR}$ ). We believe that, among all ESF components, LUB is likely the main component bound to the underlying FN. Although BSA is expected to adsorb first onto the FN layer, after 1 h of incubation, ESF molecules with higher affinity, such as LUB ( $K_d = 0.12$  nM<sup>46</sup>), can easily exchange with BSA. LUB is usually found at concentrations of 0.05–0.2 mg/mL in SF, that is, higher than the LUB concentration used in our experiments, which would further enhance its binding kinetics.<sup>46</sup> Higher  $M_w$  molecules such as HA have smaller diffusion constants and would need to possess a higher binding constant in order to replace LUB. Additionally, LUB molecules from SF were previously reported to be decorated with PL, a mechanism that has been proposed to aid in the transport of PL toward the superficial zone of cartilage.<sup>65,66</sup> The presence of similar LUB-PL complexes adsorbed from ESF could explain the larger brush length values we measured in the FN+ESF system. Finally, our brush lengths for both FN+LUB and FN+ESF are smaller than the one reported for pure LUB adsorbed on mica ( $L = 65$  nm).<sup>18</sup> Figure 6 describes the concentration-dependent mechanism we propose for LUB binding (and overall LUB coverage) onto FN films. Briefly, LUB molecules adsorbed from low concentration solutions have shown shorter interaction distances as compared to those adsorbed from higher concentration solutions.<sup>18</sup> In our model, low LUB concentration would increase the distance between the FN-bound PEX-like domains, building LUB loops with larger radii of curvature to maximize surface coverage. Such configuration

would lead to better wear protection and would be manifested as shorter-range interaction. In contrast, when adsorbed from ESF, that is, at high LUB concentration, the smaller distance between PEX-like domains would lead to loops with smaller radii of curvature (hence covering smaller surface areas), which would result in increased brush length values. This proposed mechanism would also account for the shorter interaction distances we found for FN+LUB (and LUB from ESF, FN+ESF) with respect to the values reported for LUB only by Zappone et al.<sup>17</sup> (see Table 3).

Our normal forces data also show that FN was able to tether HA to mica, as indicated by larger long-range brush lengths ( $L_{LR}$ ) found in FN+HA layers (with respect to FN only), which were similar to those reported for HA grafted onto mica with APTES.<sup>23</sup>  $L_{SR}$  fitting values were attributed to the bending and flattening of HA molecules at the surface. These values derive from the long linear structure and high  $M_w$  of HA (relative to the other SF components, see Table 2) combined with its high degree of hydration. The binding mechanisms of HA to cartilage surfaces are still unclear. In our study, the underlying FN film did not possess either the right degree of porosity or the external mechanical stimuli needed to mechanically trap HA molecules, as believed for full cartilage.<sup>20</sup> Hence, we suggest that FN-HA tethering likely occurs through electrostatic interactions between some of the multiple carboxylic acids available on HA and amine groups carried by the numerous lysines on FN.

Finally, in the presence of concentrated BSA, the resulting FN+BSA film thickness was smaller than that of FN alone. We attribute this film collapse to the exposure of hydrophobic sites on FN induced by the presence of BSA, which led to further unfolding of FN type III modules. BSA is known for its high affinity toward hydrophobic sites and is often used to “passivate” surfaces as a blocker of nonspecific (e.g., hydrophobic) interactions. Another explanation for the FN+BSA film collapse could be desorption of FN from the mica substrate and its exchange with BSA molecules; however, such a mechanism is improbable because of both the larger  $M_w$  of FN and its initial unfolding at the mica surface (leading to enhanced interfacial adhesion).

**Role of FN in Friction and Wear Protection.** Friction forces and wear protection varied greatly among the different SF layers physisorbed onto FN. In contrast with the other systems, in the FN+LUB wearless friction case, coefficients of friction increased as a function of shear velocity, likely due to shear thickening of the system. The molecular origin of such shear thickening could be due either to the stretching of existing FN-LUB or LUB-LUB bonds, or to the shear-induced formation of strong noncovalent bonds between proteins (as it is quite common in biological fluids). FN+LUB coefficients of friction also fell into the range of values previously reported for LUB alone on mica at high loads.<sup>18</sup> However, in our study, neither the aggregation (or removal) of FN and LUB molecules nor the damage of the mica substrate was ever observed, even when the system was subjected to pressures up to 4 MPa (reaching 14 MPa at the highest shearing velocity tested). The remarkable wear protection exhibited by LUB was attributed to the strong binding between FN and LUB through its PEX-like domain. This complements the efficient brush-against-brush lubrication provided by the highly hydrated layers surrounding the exposed negatively charged mucin-like domain of LUB that prevent brush interpenetration. It is worth pointing out that these wearless

experiments were carried out using low LUB concentration (0.02 mg/mL), suggesting that both the optimization of LUB's binding configuration and the maximization of its surface coverage onto FN lead to more robust wear protection. This idea is in agreement with previous studies reporting that both wear protection and friction forces are highly sensitive to LUB concentration.<sup>18,26,43</sup>

Although they exhibited the highest friction coefficients among all tribosystems studied, FN+ESF films provided effective wear protection of surfaces (similar to that observed for FN+LUB films). This finding reaffirms that coefficients of friction and wear protection are not necessarily related to each other.<sup>22</sup> In contrast with the FN+LUB film, the confined FN+ESF film showed significant structural changes under shear. MBI spectroscopy revealed material accumulation (likely weakly bound HA, PL, and BSA forming agglomerates) at the edges of the shearing junction, while strongly bound LUB acted as an efficient lubricant. However, these structural changes in the FN+ESF film never generated damage to the underlying mica substrate, even under pressures up to 4 MPa. Similar observations have been reported when shearing SF, where gel abrasion and particle formation have been proposed as the mechanisms behind the onset of the lamina splendens formation.<sup>32</sup> In fact, among all macromolecules present in SF, LUB is the one that has been widely acknowledged to act as a good boundary lubricant. Our results are in agreement with work by Elsaïd<sup>46</sup> and co-workers who showed that, among all molecules present in the extracellular matrix of articular cartilage, the highest affinity of LUB is toward FN.

In contrast, FN+HA films display high coefficients of friction, both before and after the occurrence of wear. This result was expected, as it has previously been shown that HA alone is an insufficient boundary lubricant.<sup>22</sup> This is probably a consequence of poor interpenetration resistance. The onset of wear could then result from the entanglement of HA molecules, tightly bound to the FN-coated mica, leading to the cleavage of the underlying mica substrates.<sup>23,26,67</sup>

When adsorbed onto hydrophilic surfaces (such as mica), BSA builds a dense and thick boundary layer that provides low coefficients of friction, as observed on ceramic surfaces.<sup>38</sup> However, in our experiments, mica has been previously coated with multimodular and flexible FN that easily unfolds to expose (otherwise hidden) hydrophobic sites to BSA. Additionally, the denatured (unfolded) proteins are less efficiently hydrated and usually act as poor boundary lubricants.

Finally, it is important to keep in mind that our model systems utilize stiff and nonporous confining surfaces (mica), while natural cartilage is compliant and highly porous. Thus, joint lubrication is more complex and is likely controlled by multiple lubrication mechanisms, each of them being efficient under a certain range of shearing conditions. At high loads and low shearing velocities, ESF molecules build a gel layer that acts as an effective boundary lubricant able to maintain separation between opposing cartilage surfaces, while at higher shearing velocities, hydrodynamic lubrication plays a major role,<sup>55</sup> confirming that joint lubrication is an intrinsically adaptive process.

## CONCLUSIONS

Collectively, our results suggest that FN acts as an efficient tethering component for boundary lubricant molecules such as LUB, which in turn enhances the protection of the underlying shearing mica surfaces against abrasive wear. More specifically,

our normal force measurements indicate that FN strongly binds to LUB and HA and that the resulting films can be described as purely repulsive effective brush layers (Alexander-de Gennes theory) adsorbed onto mica surfaces, as indicated by reversible long-range repulsive forces between surfaces. Additionally, our tribological measurements demonstrate that, among all ESF components, FN and LUB synergistically ensure the lowest friction and provide the most efficient protection of the shearing mica surfaces against damage, as suggested by the structural robustness of FN+LUB films when subjected to a wide range of shearing velocities and pressures up to about 14 MPa, that is, above the physiological range. These findings may have important implications for our understanding of diseased joints, such as those affected by osteoarthritis where FN is up-regulated, LUB down-regulated, and HA cleaved. This dysregulation in joint homeostasis could then facilitate the binding of more HA (or SA) at the expense of LUB (given that HA or SA are present at much higher concentrations than LUB in ESF), which requires detailed investigation.

## ■ ASSOCIATED CONTENT

### **S Supporting Information**

Figure S1 shows semilog plots of ESF and BSA in absence of underlying FN. Figure S2 shows friction force as a function of normal force between mica surfaces with either adsorbed ESF or adsorbed BSA. Figure S3 shows debris size measured as a function of normal force. The Supporting Information is available free of charge on the [ACS Publications website](#) at DOI: [10.1021/acs.biomac.5b00810](https://doi.org/10.1021/acs.biomac.5b00810).

(PDF)

## ■ AUTHOR INFORMATION

### Corresponding Author

\*E-mail: [dg434@cornell.edu](mailto:dg434@cornell.edu). Tel.: +1 (607) 255-1623.

### Notes

The authors declare no competing financial interest.

## ■ ACKNOWLEDGMENTS

This research was supported by the NSF under Award DMR-1352299 (to D.G.), CONACYT under Award 308671 (to R.C.A.E.), the Cornell Center for Materials Research through Award Number (NSF DMR-1120296), and the Cornell University Biotechnology Resource Center (BRC) for data collected on the Zeiss LSM 710 Confocal (NIH 1S10RR025502-01). We also thank Dr. Kirk J. Samaroo, Dr. Mingchee Tan, Edward Bonnevie, Heidi Reesink, and Prof. Dave Putnam for enriching discussions.

## ■ REFERENCES

- Wright, V.; Dowson, D. *J. Anat.* **1976**, *121* (1), 107–118.
- Forster, H.; Fisher, J. *Proc. Inst. Mech. Eng., Part H* **1996**, *210*, 109–119.
- Morrell, K. C.; Hodge, W. A.; Krebs, D. E.; Mann, R. W. *Proc. Natl. Acad. Sci. U. S. A.* **2005**, *102* (41), 14819–14824.
- McCutchen, C. W. *Wear* **1962**, *5*, 1–17.
- Mow, V. C.; Lai, M. *SIAM Rev.* **1980**, *22* (3), 275–317.
- Radin, E. L.; Swann, D. A.; Weisser, P. A. *Nature* **1970**, *228*, 377–378.
- Hughes, L. C.; Archer, C. W.; ap Gwynn, I. *Eur. Cell. Mater.* **2005**, *9*, 68–84.
- Dédinaité, A. *Soft Matter* **2012**, *8* (2), 273.
- MacConail, M. A. *J. Bone Jt. Surg.* **1951**, *33B* (2), 251–257.
- Jurvelin, J. S.; Müller, D. J.; Wong, M.; Studer, D.; Engel, A.; Hunziker, E. B. *J. Struct. Biol.* **1996**, *117* (1), 45–54.
- Jeffery, A.; Blunn, G.; Archer, C.; Bentley, G. *J. Bone Jt. Surg.* **1991**, *73* (5), 795–801.
- Teshima, R.; Otsuka, T.; Takasu, N.; Yamagata, N.; Yamamoto, K. *J. Bone Jt. Surg.* **1995**, *77-B*, 460–464.
- Balazs, E. A. *Struct. Chem.* **2009**, *20* (2), 233–243.
- Hills, B. A. *Intern. Med. J.* **2002**, *32*, 242–251.
- Hills, B. A.; Crawford, R. W. *J. Arthroplasty* **2003**, *18* (4), 499–505.
- Fan, J.; Myant, C.; Underwood, R.; Cann, P. *Faraday Discuss.* **2012**, *156*, 69.
- Swann, D. A.; Silver, F. H.; Slayter, H. S.; Stafford, W.; Shore, E. *Biochem. J.* **1985**, *225* (1), 195–201.
- Zappone, B.; Ruths, M.; Greene, G. W.; Jay, G. D.; Israelachvili, J. N. *Biophys. J.* **2007**, *92* (5), 1693–1708.
- Zappone, B.; Greene, G. W.; Oroodjev, E.; Jay, G. D.; Israelachvili, J. N. *Langmuir* **2008**, *24* (4), 1495–1508.
- Greene, G. W.; Banquy, X.; Lee, D. W.; Lowrey, D. D.; Yu, J.; Israelachvili, J. N. *Proc. Natl. Acad. Sci. U. S. A.* **2011**, *108* (13), 5255–5259.
- Tadmor, R.; Chen, N.; Israelachvili, J. N. *Macromolecules* **2003**, *36* (25), 9519–9526.
- Lee, D. W.; Banquy, X.; Das, S.; Cadirov, N.; Jay, G.; Israelachvili, J. N. *Acta Biomater.* **2014**, *10* (5), 1817–1823.
- Yu, J.; Banquy, X.; Greene, G. W.; Lowrey, D. D.; Israelachvili, J. N. *Langmuir* **2012**, *28* (4), 2244–2250.
- Sorkin, R.; Kampf, N.; Dror, Y.; Shimoni, E.; Klein, J. *Biomaterials* **2013**, *34* (22), 5465–5475.
- Chang, D. P.; Abu-lail, N. I.; Coles, J. M.; Guilak, F.; Jay, G. D.; Zauscher, S. *Soft Matter* **2009**, *5* (18), 3438–3445.
- Das, S.; Banquy, X.; Zappone, B.; Greene, G. W.; Jay, G. D.; Israelachvili, J. N. *Biomacromolecules* **2013**, *14*, 1669–1677.
- Chang, D. P.; Guilak, F.; Jay, G. D.; Zauscher, S. *J. Biomech.* **2014**, *47* (3), 659–666.
- Liu, C.; Wang, M.; An, J.; Thormann, E.; Dédinaité, A. *Soft Matter* **2012**, *8* (40), 10241.
- Seror, J.; Sorkin, R.; Klein, J. *Polym. Adv. Technol.* **2014**, *25* (5), 468–477.
- Seror, J.; Merkher, Y.; Kampf, N.; Collinson, L.; Day, A. J.; Maroudas, A.; Klein, J. *Biomacromolecules* **2012**, *13* (11), 3823–3832.
- Schmidt, T. A.; Gastelum, N. S.; Nguyen, Q. T.; Schumacher, B. L.; Sah, R. L. *Arthritis Rheum.* **2007**, *56* (3), 882–891.
- Banquy, X.; Lee, D. W.; Das, S.; Hogan, J.; Israelachvili, J. N. *Adv. Funct. Mater.* **2014**, *24*, 3152–3161.
- Balazs, E. A.; Watson, D.; Duff, I. F.; Roseman, S. *Arthritis Rheum.* **1967**, *10* (4), 357–376.
- Bensouyad, A.; Hollander, A. P.; Dularay, B.; Bedwell, A. E.; Cooper, R. A.; Hutton, C. W.; Dieppe, P. A.; Elson, C. J. *Ann. Rheum. Dis.* **1990**, *49* (5), 301–307.
- Herbert, K. E.; Coppock, J. S.; Griffiths, A. M.; Williams, A.; Robinson, M. W.; Scott, D. L. *Ann. Rheum. Dis.* **1987**, *46* (10), 734–740.
- Jay, G. D.; Haberstroh, K.; Cha, C. J. *J. Biomed. Mater. Res.* **1998**, *40* (3), 414–418.
- Davis, W. H.; Lee, S. L.; Sokoloff, L. *J. Biomech. Eng.* **1979**, *101* (3), 185–192.
- Heuberger, M. P.; Widmer, M. R.; Zobeley, E.; Glockshuber, R.; Spencer, N. D. *Biomaterials* **2005**, *26* (10), 1165–1173.
- Schmidt, T. A.; Sah, R. L. *Osteoarthritis Cartilage* **2007**, *15* (1), 35–47.
- Mabuchi, K.; Obara, T.; Ikegami, K.; Yamaguchi, T.; Kanayama, T. *Clin. Biomech.* **1999**, *14* (5), 352–356.
- Swann, D. A.; Sotman, S.; Dixon, M.; Brooks, C. *Biochem. J.* **1977**, *161* (3), 473–485.
- Swann, D. A.; Slayter, H. S.; Silver, F. H. *J. Biol. Chem.* **1981**, *256* (11), 5921–5925.
- Gleghorn, J. P.; Jones, A. R. C.; Flannery, C. R.; Bonassar, L. J. *J. Orthop. Res.* **2009**, *27* (6), 771–777.

- (44) Jay, G. D. *Connect. Tissue Res.* **1992**, *28*, 71–88.
- (45) Jones, A. R. C.; Gleghorn, J. P.; Hughes, C. E.; Fitz, L. J.; Zollner, R.; Wainwright, S. D.; Caterson, B.; Morris, E. A.; Bonassar, L. J.; Flannery, C. R. *J. Orthop. Res.* **2007**, *25* (3), 283–292.
- (46) Elsaid, K. A.; Chichester, C. O.; Jay, G. D. *Trans. Orthop. Res. Soc.* **2007**, *32*, 551.
- (47) Nishida, K.; Inoue, H.; Murakami, T. *Ann. Rheum. Dis.* **1995**, *54* (12), 995–998.
- (48) Nakashima, K.; Sawae, Y.; Murakami, T. *JSME Int. J., Ser. C* **2005**, *48* (4), 555–561.
- (49) Chevalier, X. *Semin. Arthritis Rheum.* **1993**, *22* (5), 307–318.
- (50) Burton-Wurster, N.; Horn, V. J.; Lust, G. *J. Histochem. Cytochem.* **1988**, *36* (6), 581–588.
- (51) Smith, M. L.; Gourdon, D.; Little, W. C.; Kubow, K. E.; Eguiluz, R. A.; Luna-Morris, S.; Vogel, V. *PLoS Biol.* **2007**, *5* (10), e268.
- (52) Israelachvili, J. N. *J. Colloid Interface Sci.* **1973**, *44* (2), 259–272.
- (53) Gourdon, D.; Yasa, M.; Alig, A. R. G.; Li, Y.; Safinya, C. R.; Israelachvili, J. N. *Adv. Funct. Mater.* **2004**, *14* (3), 238–242.
- (54) Israelachvili, J. N. *Intermolecular and Surface Forces*; Academic Press and Elsevier: Amsterdam, 2011.
- (55) Klein, J. *Proc. Inst. Mech. Eng., Part J* **2006**, *220*, 691–710.
- (56) Seror, J.; Merkher, Y.; Kampf, N.; Collinson, L.; Day, A. J.; Maroudas, A.; Klein, J. *Biomacromolecules* **2011**, *12* (10), 3432–3443.
- (57) Elter, P.; Lange, R.; Beck, U. *Colloids Surf., B* **2012**, *89*, 139–146.
- (58) Klotzsch, E.; Smith, M. L.; Kubow, K. E.; Muntwyler, S.; Little, W. C.; Beyeler, F.; Gourdon, D.; Nelson, B. J.; Vogel, V. *Proc. Natl. Acad. Sci. U. S. A.* **2009**, *106* (43), 18267–18272.
- (59) Wan, A. M. D.; Schur, R. M.; Ober, C. K.; Fischbach, C.; Gourdon, D.; Malliaras, G. G. *Adv. Mater.* **2012**, *24* (18), 2501–2505.
- (60) Wu, F.; Lin, D. D. W.; Chang, J. H.; Fischbach, C.; Estroff, L. A.; Gourdon, D. *Cryst. Growth Des.* **2015**, *15* (5), 2452–2460.
- (61) Bingham, R. J.; Meenan, N. A.; Schwarz-Linek, U.; Turkenburg, J. P.; Garman, E. F.; Potts, J. R. *Proc. Natl. Acad. Sci. U. S. A.* **2008**, *105* (34), 12254–12258.
- (62) Little, W. C.; Schwartlander, R.; Smith, M. L.; Gourdon, D.; Vogel, V. *Nano Lett.* **2009**, *9* (12), 4158–4167.
- (63) Pankov, R. *J. Cell Sci.* **2002**, *115* (20), 3861–3863.
- (64) Estrella, R. P.; Whitelock, J. M.; Packer, N. H.; Karlsson, N. G. *Biochem. J.* **2010**, *429* (2), 359–367.
- (65) Hills, B. A. *Proc. Inst. Mech. Eng., Part H* **2000**, *214* (1), 83–94.
- (66) Coles, J. M.; Zhang, L.; Blum, J. J.; Warman, M. L.; Jay, G. D.; Guilak, F.; Zauscher, S. *Arthritis Rheum.* **2010**, *62* (6), 1666–1674.
- (67) Chen, Y. L.; Israelachvili, J. N. *Science (Washington, DC, U. S.)* **1991**, *252* (5009), 1157–1160.